49th AIAA Aerospace Sciences Meeting including the New Horizons Forum and Aerospace Exposition
4 - 7 January 2011, Orlando, Florida
AIAA 2011-954

Experimental Study of a DBD-Plasma Driven Channel Flow

Marco Debiasi[1] and Li Jiun-Ming[2]
Temasek Laboratories, National University of Singapore, Singapore, 117411

A DBD-plasma driven channel flow is proposed and studied experimentally. The configuration consists of two DBD plasma actuators mirroring each other on opposite wall of a channel. The rationale is that a stronger flow could be obtained by merging the wall jets created by the mirroring DBD plasma actuator. Measurements of the velocity of the channel flow so obtained for different values of the separation of the walls have been performed with a miniature pitot probe mounted on a micro-step 3D traverse system. The data are compared with the corresponding ones for wall jets induced by a single DBD plasma actuator. The preliminary results obtained suggest that DBD-plasma driven channel flows could be used to create a non-continuous small suction device or a small jet as demanded by flow control applications.

Nomenclature

f	=	frequency
F	=	force
h	=	channel height (distance between the upper and lower surfaces of the channel)
I	=	current
$\dot{m}$	=	mass flow rate
M	=	Mach number
p	=	pressure
u	=	velocity in the x direction
u_{max}	=	maximum value of the velocity in the x direction
V	=	voltage
V_{pp}	=	peak-to-peak voltage of sinusoidal signal
x	=	streamwise coordinate downstream of the exposed electrode
x_{max}	=	distance between the exposed electrode and the exit of the channel
w	=	channel width (in the spanwise direction)
z	=	normal coordinate

Greek letters

ρ	=	air density

I. Introduction

ACTIVE airflow control consists of manipulating a flow to affect a desired change. For example, efficient flow control systems could modify the laminar-turbulent transition inside the boundary layer, prevent or induce separation, reduce the drag and enhance the lift of airfoils, stabilize or mix airflow in order to avoid unsteadiness which generates unwanted vibrations, noise and energy losses. This is of large technological importance for industries where internal and external airflows occur, and more specifically for aeronautics.

Among all the active control methods, a recent technology using non-thermal dielectric barrier discharge (DBD) plasmas is in full expansion. Indeed, although more conventional mechanical devices may be effective, they have some drawbacks. In particular they add weight and /or volume, they may be complicated, and they are potential sources of noise and vibration. Moreover, their components are subject to wear and may break down. In contrast, plasma actuators do not exhibit all these drawbacks.

[1] Senior Research Scientist, Temasek Laboratories, National University of Singapore, Singapore, Member AIAA.
[2] Research Scientist, Temasek Laboratories, National University of Singapore, Singapore.

A DBD plasma actuator consists of two electrodes separated by a dielectric barrier. When a high voltage, alternating current is applied, the local air is ionized. The ions collide with the surrounding neutral particles so as to transfer their momentum to the air.[1] Therefore, the plasma actuator can be thought of as imposing a localized body force to the surrounding air. The aim of using this electric wind is in most cases to accelerate the airflow tangentially and very close to the wall in order to modify the airflow profile within the boundary layer. The main advantage of this process is its direct conversion of electric energy into kinetic energy without involving moving mechanical parts. Thus it may be considered to be a very simple type of MEMS. Secondly, its response time is very short and enables real-time control at high frequency. Its main disadvantage is the low efficiency of energy conversion currently achievable.

The advantages of robustness, simplicity, stability, low power consumption and the ability of real-time control of these systems make them desirable candidates for applications in aeronautics.[1] The application of DBD plasma actuators for aerodynamic flow control was pioneered by Roth's group in the University of Tennessee at the end of the 1990s. Their studies showed that the DBD-based actuator, called OAUGDP, could induce airflow with velocity up to a few m/s that have considerable influence on flow control and flow attachment to airfoils.[2-5] Numerous recent researches have studied the physical mechanisms[6-23] and the use of DBD plasma actuators, especially for aerodynamic flow control.[1,24-39] To date, there are more than 30 groups studying this subject mostly in the USA, Europe, and Japan. The major research groups are at the University of Tennessee, the University of Notre Dame, the US Air Force Academy, and the University of Poitiers.

The main scope of this project is to explore the characteristics of the flow induced by two DBD plasma actuators mirroring each other on opposite walls of a channel. The rationale for this configuration, which at the best knowledge of the authors has not yet been investigated experimentally,[40] is that, at sufficiently small values of the walls' separation, the wall jets created by the mirroring actuators should merge into a stronger flow filling the channel. Initial measurements of the channel flow's velocity for different values of the walls' separation have been obtained with a miniature pitot probe mounted on a micro-step 3D traverse system. The data are compared with the corresponding ones for wall jets induced by a single DBD plasma actuator.

II. Experimental Setup

A schematic diagram and some pictures of the experimental setup are shown in Figs. 1 and 2, respectively.

This consists of a channel with lower and upper walls of width w = 90 mm each embedding a DBD plasma actuators. These walls are sandwiched between two side walls with slots that allow adjusting the distance between the lower and the upper wall, i.e. the channel height h, in the range of 2 to 30 mm. The nominal values of h explored in this study are 2, 3, 4, 5, 6, 8, 10, 20, 30 mm and ∞ which corresponds to the case of a single DBD plasma actuator open to the ambient. All the walls are made of 15mm thick Plexiglass. The walls at the entrance of the channel are contoured so to minimize the contraction of the flow and the associated losses.

Each DBD plasma actuator is flush mounted in a recess of the wall which spans the whole width of the channel. The actuators were fabricated by using copper clad PCB laminates with uniform relative permittivity (2.2 at 10 GHz) and low dissipation factor (0.0009 at 10 GHz). The dielectric material of the laminates is 1.5 mm-thick PTFE coated woven fiberglass fabric and the electrodes' material is 18 μm-thick electrodeposited copper. The exposed (upstream) electrode is 8 mm long in the streamwise direction and 80 mm wide in the spanwise direction, Fig. 2 b). The buried electrode, indicated by dashed lines in Fig. 2 b), has same width and is 15 mm long. To ensure that the discharge occurs only on the exposed surface, the buried electrode is covered by a layer of Kapton sheet.

The electrical circuit of the setup is shown in Fig. 1. A sinusoidal high voltage is applied to the exposed electrodes of the two actuators whereas the buried electrodes are grounded. The voltage is provided by a PVM500 plasma driver. This plasma driver can produce an output voltage up to a maximum of 40 kV (depending on the loading). There is no provision for an input signal and the output signal waveform is only sinusoidal in the frequency range from 20 to 30 kHz. However there is an adjustable duty cycle, which allows delivering different power output (maximum 200 watts). The PVM500 unit allows the users to tune a capacitive load within the range of 25 to 200 pF. This feature is to diminish the reactive components so to deliver the maximum power to the load (impedance matching). A safety shutdown circuit prevents overload of the driver in case of circuit breakdown. In this study, we apply two voltages of 8 kV_{pp} and 12 kV_{pp} at a frequency of 25 kHz. Although the frequency is slightly higher than those explored by other groups, it is still meaningful.

The actual voltage at the exit of the plasma driver and across the DBD plasma actuators is measured with a Tektronix P6015A high-voltage probe. The probe includes a compensation unit through which the signal is passed to the measuring device and a ground clip that is connected to the ground point of the circuit under test. The current

through each DBD plasma actuator is obtained by measuring the voltage across a 75 Ω resistor in series with the grounded electrode. The voltage and current signals are observed and recorded simultaneously through a Tektronix TDS2024B oscilloscope which is able to collect 2000 samples per channel at a frequency up to 2 MHz. Such a high sampling frequency is necessary to resolve the spikes of the current signal.

A miniature pitot probe schematized in Fig. 1 was used to perform steady pressure measurements on the flow induced downstream of the actuators. The diameter of the opening in the tip of the pitot probe is 0.69 mm. This small pitot probe was mounted on a micro-step 3D traverse system that allows step increments as small as 2 μm along its three axes. In the current study we surveyed the flow characteristics at various x (streamwise) locations downstream of the exposed electrodes along the channel centerline by scanning the flow in the z direction (normal to the actuator surface). To avoid arching to the probe tip, the minimum downstream distance is x = 15 mm. Steps increments Δz = 0.25 mm were used close to the walls (z < 4.25 mm) whereas larger increments Δz = 0.5 mm were used at larger distances. The pitot probe was connected to a Setra model 264 pressure transducer capable of measurements in the 0 to 249 Pa range. The transducer was calibrated before and after each set of experiments and the calibration parameters were used in the processing of the pitot data. The voltage from the transducer was acquired at 10 kHz by a National Instruments PXI6122 multifunction DAQ board. This board also controlled the movements of the 3D traverse system. The typical sequence for the data acquisition at each point of the flow consisted of moving the tip of the pitot probe to this point, wait for 1 second for settling of the pressure in the pitot system, trigger the acquisition of the voltage and current signals through the oscilloscope and acquire a pressure signal of 1-second duration, then record all the signals in a designated file. The waiting time extended to 4 seconds close to the walls since here the pressure settling took longer, especially close to the actuator. All the velocity measurements were conducted in a protected environment so to eliminate any external flow (e.g. due to room ventilation or to the movement of people) which could adversely affect the small flow velocities measured.

III. Results

Figure 3 shows the velocity profiles $u(x,z)$ measured by scanning the flow in the z direction (normal to the actuator surface) at different locations x downstream of the exposed electrode for the case of a single DBD plasma actuator open to the ambient and operating at 8 kV_{pp}. This configuration corresponds to lower surface of a channel with infinite distance between the upper and lower surfaces ($h = \infty$). At x = 15 mm, the closest location to the exposed electrode at which the tip of the pitot probe can be placed without risk of arching, the maximum velocity value is about 2.0 m/s. The velocity reduces and its profile broadens moving downstream. Overall the velocity profiles resemble those of a wall jet. Analogous profiles are shown in Fig. 4 for the actuator operating at 12 kV_{pp}. In this case the higher voltage applied to the actuator produces a wall jet with higher velocity values. The maximum velocity measured at x = 15 mm is about 4.9 m/s.

Figure 5 shows the velocity profiles $u(z)$ measured at x = 63 mm for different values of the channel height h with the lower and upper actuators operating at 12 kV_{pp}. The downstream location x = 63 mm is as close to the exposed electrodes as the tip of the miniature pitot probe can reach from the channel exit, Fig 1. For the case of $h = \infty$ the downstream distance is actually x = 60 mm (the same profile is shown in Fig. 4). The discrepancy between these values of x is considered inconsequential for the scope of this analysis. At h = 30 mm the lower and upper actuators operating at 12 kV_{pp} appear to produce distinct wall jets that have minimal combined effect on the flow, as indicated by half of the velocity profile for h = 30 mm being very similar to the profile observed with $h = \infty$. As h decreases the wall jets progressively merge by gradually filling and then increasing the center of the velocity profile until this approaches a shape similar to a Poiseuille flow. For the same configurations Fig. 6 shows the velocity profiles measured at the exit of the channel (x_{max} = 86 mm) for which analogous observations can be made. Velocity profiles analogous to those in Figs. 5 and 6 were obtained with the actuators operating at 8 kV_{pp}. For the sake of brevity these are not shown here as they show similar features but with overall lower velocity values.

Figures 7 and 8 plot the maximum values of the velocity profiles u_{max} versus the channel height h. Figure 7 shows that at 12 kV_{pp} the maximum velocity measured at x = 63 mm increases with decreasing h and reaches a value about twice that of the wall jet produced by a single DBD plasma actuator ($h = \infty$). The value of u_{max} obtained at h = 30 mm is lower than that at $h = \infty$ which we believe can be corrected by statistical analysis with additional velocity measurements (see also Fig. 5 for $h = \infty$ and 30 mm). At 8 kV_{pp} the maximum velocity is lower and does not increase with decreasing h but rather reaches a maximum at h = 4 mm. This suggests that, for a given length of the channel, the flow viscosity becomes increasingly dominant with decreasing the channel height, an effect that, at this voltage, balances and eventually reduces the raise of u_{max} obtained by decreasing the distance between the lower and upper actuators. Figure 8 shows the data obtained at x_{max} = 86 mm. For actuation at 12 kV_{pp} the largest value of u_{max}

is obtained with h = 3 mm. This is about twice the value obtained in the same conditions with $h = \infty$. Further decreasing the channel height does not seem to benefit u_{max} , possibly due to the increasing effect of the flow viscosity with increasing the x/h ratio. Similarly, decreasing h for actuation at 8 kV_{pp} initially produces a moderate increase of u_{max} followed by a drop of its value at smaller values of h. The trends observed in Fig. 8 appear to be consistent with the antagonist effects that the flow viscosity and the proximity of the lower and upper actuator have on the flow velocity with reducing the channel height.

The mass flow rate per unit span $\dot{m}_w$ of the channel is calculated from the profiles in Figs. 3 to 6 as:

$$\dot{m}_w \equiv \frac{\dot{m}}{w} = \rho \int_0^h u(z)dz \tag{1}$$

where ρ is the density of the air at ambient conditions. Figures 9 plots the mass flow rate per unit span of the wall jets created by a single DBD plasma actuator, i.e. the values of the mass flow rate obtained with Eq. 1 from the velocity profiles of Figs. 3 and 4. As expected the mass flow rate increases with the distance x downstream of the exposed electrode as a result of the entrainment of ambient air by the wall jet. Similarly, Fig. 10 shows the values of $\dot{m}_w$ of the DBD-plasma-driven channel flows versus the channel height h. For large values of h (30 and 20 mm) the channel flows at both actuation voltages have about twice as much mass flow rate compared to the corresponding wall jets. This is consistent with the previous observation that at large values of h the lower and upper actuators of the channel produce two distinct wall jets. With reducing h the mass flow rate decreases as the channel becomes narrower.

The rate of the flow momentum per unit span of the channel, i.e. the force per unit span of the channel F_w is calculated from the profiles in Figs. 3 to 6 as:

$$F_w \equiv \frac{F}{w} = \rho \int_0^h u^2(z)dz \tag{2}$$

Figure 11 shows the values of F_w obtained for the wall jets and for the DBD-plasma-driven channel flows at x = 63 mm downstream of the exposed electrode. Similar to the case of the mass flow rate, F_w at large values of h is about twice that of the wall jet measured at the same location. For h < 10 mm F_w drops quickly as a result of the decreased mass flow rate in the channel. Similar trends can be observed for F_w obtained at x_{max} = 86 mm in Fig. 12. Even though the force per unit span rapidly decreases with h, it is interesting to note that, at least for actuation at 12 kV_{pp}, the force per unit span of the channel flow is greater or about equal to that of the wall jet for all but the smallest channel height of 2 or 3 mm. This indicates that, in spite of its reduced mass flow rate, the channel configuration is capable of producing a useful momentum concentrated in a narrow flow.

IV. Conclusion

Initial measurements of the flow velocity induced by DBD plasma actuators mounted on the opposite walls of a channel have been acquired and analyzed. Velocity profiles were obtained with a miniature pitot probe at two locations downstream of the exposed electrodes for different values of the separation between the opposite walls. From these the mass flow rate and the force per unit span of the channel were calculated. The results are compared with the corresponding values of wall jets induced by a single DBD plasma actuator, the typical configuration for this type of device. The results indicate that at large values of the separation between the opposite actuators these produce independent wall jets. As the separation decreases the wall jets merge and create a flow resembling the Poiseuille type. The merged flow in the channel has a velocity about twice that of the corresponding wall jet. The mass flow rate of the channel rapidly decreases with the wall separation. However the force exerted by the flow per unit span of the channel remains comparable to that of the corresponding wall jet except for the smallest values of wall separation. When the separation between the walls becomes too small, the flow viscosity becomes increasingly dominant which balances or reduces the raise of the flow velocity obtained by decreasing the separation between the DBD plasma actuators.

Additional measurements for this type of flow will be carried out in the future by using particle image velocimetry (PIV) to capture the velocity flow field and by using hot-wire measurements to time-resolve the

fluctuations of the flow velocity at selected locations of the channel. At the same time, a larger spectrum of actuation voltages and frequencies will be explored.

It is anticipated that the effectiveness of the channel flow proposed in this study could be increased by using a series of phased DBD plasma actuators on the opposite walls of the channel. A device of this type could be used to create a non-continuous small suction device or a small jet as demanded by flow control applications.

Acknowledgments

The authors would like to thank Mr. Tan Peng Khiang for his assistance in manufacturing the DBD plasma actuators.

References

[1]Moreau, E., "Airflow control by non-thermal plasma actuators," *Journal of Physics D: Applied Physics*, Vol. 40, No. 3, 2007, pp. 605-636.

[2]Roth, J. R. , Sherman, D. M., and Wilkinson, S. P., "Boundary layer flow control with a one atmosphere uniform glow discharge surface plasma," AIAA paper 98-0328, *36th AIAA Aerospace Sciences Meeting and Exhibit*, Reno, NV, 1998.

[3]Roth, J. R., "Electrohydrodynamically induced airflow in a one atmosphere uniform glow discharge surface plasma," *25th IEEE Int. Conf. Plasma Science*, 1998.

[4]Roth, J. R., Sherman, D. M., and Wilkinson, S. P., "Electrohydrodynamic Flow Control with a Glow-Discharge Surface Plasma," *AIAA Journal*, Vol. 38, No. 7, 2000, pp. 1166-1172.

[5]Roth, J. R., "Aerodynamic flow acceleration using paraelectric and peristaltic electrohydrodynamic effects of a one atmosphere uniform glow discharge plasma," *Physics of Plasma*, Vol. 10, No. 5, 2003, pp. 2117-2126.

[6]Roth, J. R., "Investigation of a uniform glow discharge plasma in atmospheric air," AFOSR-TR-5, 1995.

[7]Massines, F., Rabehi, A., Decomps, P., Gadri, R. B., Ségur, P., and Mayoux, C., "Experimental and theoretical study of a glow discharge at atmospheric pressure controlled by dielectric barrier," *Journal of Applied Physics*, Vol. 83, No. 6, 1998, pp. 2950-2957.

[8]Miralaï, S. F., Monette, E., Bartnikas, R., Czeremuszkin, R., Latrèche, V., and Wertheimer, M. R., "Electrical and optical diagnostics of dielectric barrier discharge (DBD) in He and N2 for polymer treatment," *Plasmas Polym.*, Vol. 5, 2000, pp. 63-77.

[9]Gherardi, N., Gouda, G., Gat, E., Ricard, A., and Massines, F., "Transition from glow silent discharge to micro-discharges in nitrogen gas," *Plasma Sources Sc. Technol.*, Vol. 9, 2000, pp. 340-346.

[10]Gherardi, N., and Massines, F., "Mechanisms controlling the transition from glow silent discharge to streamer discharge in nitrogen," *IEEE Transactions on Plasma Science*, Vol. 29, No. 3, 2001, pp. 536-544.

[11]Kogelschatz, U., "Filamentary, patterned, and diffuse barrier discharges," *IEEE Transactions on Plasma Science*, Vol. 30, No. 4, 2002, pp. 1400-1408.

[12]Chen, Z., "Impedance matching for one atmosphere uniform glow discharge plasma (OAUGDP) reactors," *IEEE Transactions on Plasma Science*, Vol. 30, No. 5, 2002, pp. 1922-1930.

[13]Enloe, C. L., McLaughlin, T. E., VanDyken, R. D., Kachner, K. D., Jumper, E. J., and Corke, T. C., "Mechanisms and responses of a single dielectric barrier plasma actuator: plasma morphology," *AIAA Journal*, Vol. 42, No. 3, 2004, pp. 589-594.

[14]Enloe, C. L., McLauglin, T. E., VanDyken, R. D., Kachner, K. D., Jumper, E. J., Corke, T. C., Post, M., and Haddad, O., "Mechanisms and responses of a single dielectric barrier plasma actuator: geometric effects," *AIAA Journal*, 2004, Vol. 42, No. 3, pp. 595-604.

[15]Ráhel', J., and Sherman, D. M., "The transition from a filamentary dielectric barrier discharge to a diffuse barrier discharge in air at atmospheric pressure," *Journal of Physics D: Applied Physics*, Vol. 38, No. 4, 2005, pp. 547-554.

[16]Iqbal, M., Corke, T. C., and Thomas, F., "Parametric optimization of single dielectric barrier discharge (sdbd) plasma actuators," *59th Annual Meeting of the APS Division of Fluid Dynamics*, November 19-21, 2006.

[17]Orlov, D. M., "Modeling and Simulation of Single Dielectric Barrier Discharge Plasma Actuators," Ph.D. Dissertation, University of Notre Dame, South Bend, IN, 2006.

[18]Fridman, A., and Cho, Y. I., *Transport phenomena in plasma*, 1st ed., Academic Press, London, 2007.

[19]Boeuf, J. P., Lagmich, Y., Unfer, T., Callegari, T., and Pitchford, L. C., "Electrohydrodynamic force in dielectric barrier discharge plasma actuators," *Journal of Physics D: Applied Physics*, Vol. 40, No. 3, 2007, pp. 652-662.

[20]Orlov, D. M., Font, G., and Edelstein, D., "Characterization of Discharge Modes of Plasma Actuators," AIAA paper 2008-1409, *46th AIAA Aerospace Sciences Meeting and Exhibit*, Reno, NV, 2008.

[21]Abe, T., Takizawa, Y., Sato, S., and Kimura, N., "Experimental study for momentum transfer in a dielectric barrier discharge plasma actuator," *AIAA Journal*, Vol. 46, No. 9, 2008, pp. 2248-2256.

[22]Jayaraman, B., Cho, Y.-C., and Shyy, W., "Modeling of dielectric barrier discharge plasma actuator," *Journal of Applied Physics*, Vol. 103, No. 053304, 2008.

[23]Balcon, N., Benard, N., Lagmich, Y., Boeuf, J.-P., Touchard, G., and Moreau, E., "Positive and negative sawtooth signals applied to a DBD plasma actuator - influence on the electric wind," *Journal of Electrostatics*, Vol. 67, No. 2-3, 2009, pp.140-145.

[24]Mohan, M. R. C., "Boundary layer flow acceleration by paraelectric and peristaltic EHD effects of aerodynamic plasma actuators," Master Thesis, The University of Tennessee, Knoxville, TN, 2004.

[25]Post, M. L., "Plasma Actuators for separation Control on stationary and oscillating airfoils," Ph.D. Dissertation, University of Notre Dame, South Bend, IN, 2004.

[26]Pons, J., Moreau, E., and Touchard, G., "Asymmetric surface dielectric barrier discharge in air at atmospheric pressure: electrical properties and induced airflow characteristics," *Journal of Physics D: Applied Physics*, Vol. 38, No. 19, 2005, pp. 3635-3642.

[27]Opaits, D. F., Roupassov, D. V., Starikovskaia, S. M., Starikovskii, A. Y., Zavialov, I. N., and Saddoughi, S. G., "Plasma Control of Boundary Layer Using Low-Temperature Non-equilibrium Plasma of Gas Discharge," AIAA paper 2005-1180, *43rd AIAA Aerospace Sciences Meeting and Exhibit*, Reno, NV, 2005.

[28]Huang, J., "Separation Control Over low pressure turbine blades using Plasma Actuators," Ph.D. Dissertation, University of Notre Dame, South Bend, IN, 2005.

[29]Roupassov, D. V., Zavialov, I. N., and Starikovskii, A. Y., "Boundary Layer Separation Plasma Control Using Low-Temperature Non-Equilibrium Plasma of Gas Discharge," AIAA paper 2006-373, *44th AIAA Aerospace Sciences Meeting and Exhibit*, Reno, NV, 2006.

[30]Roth, J. R., and Dai, X., "Optimization of the Aerodynamic Plasma Actuator as an Electrohydrodynamic (EHD) Electrical Device," AIAA paper 2006-1203, *44th AIAA Aerospace Sciences Meeting and Exhibit*, Reno, NV, 2006.

[31]Thomas, F. O., Kozlov, A., and Corke, T. C., "Plasma Actuators for Bluff Body Flow Control," AIAA paper 2006-2845, *3rd AIAA Flow Control Conference*, San Francisco, CA, 2006.

[32]Forte, M., Jolibois, J., Moreau, E., Touchard, G., and Cazalens, M., "Optimization of a Dielectric Barrier Discharge Actuator by Stationary and Non-stationary Measurements of the Induced Flow Velocity - Application to Airflow Control," AIAA paper 2006-2863, *3rd AIAA Flow Control Conference*, San Francisco, CA, 2006.

[33]Goksel, B., Greenblatt, D., Rechenberg, I., Nayeris, C. N., and Paschereit, C. O., "Steady and Unsteady Plasma Wall Jets for Separation and Circulation Control," AIAA paper 2006-3686, *3rd AIAA Flow Control Conference*, San Francisco, CA, 2006.

[34]Santhanakrishnan, A., and Jacob, J. D., "Flow control with plasma synthetic jet actuators," *Journal of Physics D: Applied Physics*, Vol. 40, No. 3, 2007, pp. 637-651.

[35]Dong, B., Bauchire, J. M., Pouvesle, J. M., Magnier, P., and Hong, D., "Experimental study of a DBD surface discharge for the active control of subsonic airflow," *Journal of Physics D: Applied Physics*, Vol. 41, No. 15, 155201, 2008.

[36]Moreau, E., Sosa, R., and Artana, G., "Electric wind produced by surface plasma actuators: a new dielectric barrier discharge based on a three-electrode geometry," *Journal of Physics D: Applied Physics*, Vol. 41, No. 11, 115204, 2008.

[37]Magnier, P., Dong, B., Hong, D., and Hureau, J., "Action of a pulsed DBD actuator on a slow jet," *Journal of Electrostatics*, Vol. 66, 2008, No. 7-8, pp. 369-374.

[38]Corke, T. C., Post, M. L., and Orlov, D. M., "Single dielectric barrier discharge plasma enhanced aerodynamics: physics, modeling and application," *Exp. Fluids*, Vol. 46, 2009, pp. 1-26.

[39]Guo, S., Burman, D., Poon, D., Mamunuru, M., Simon, T., Ernie, D., and Kortshagen, U., "Separation Control Using DBD Plasma Actuators: Designs for Thrust Enhancement," AIAA paper 2009-4184, *39th AIAA Fluid Dynamics Conference*, San Antonio, TX, 2009.

[40]Wang, C.-C., and Roy, S., "Three-Dimensional Plasma and Fluid Flow Simulation Inside a Microscale Electrohydrodynamic Pump," AIAA paper 2010-966, *48th AIAA Aerospace Sciences Meeting*, Orlando, FL, 2010.

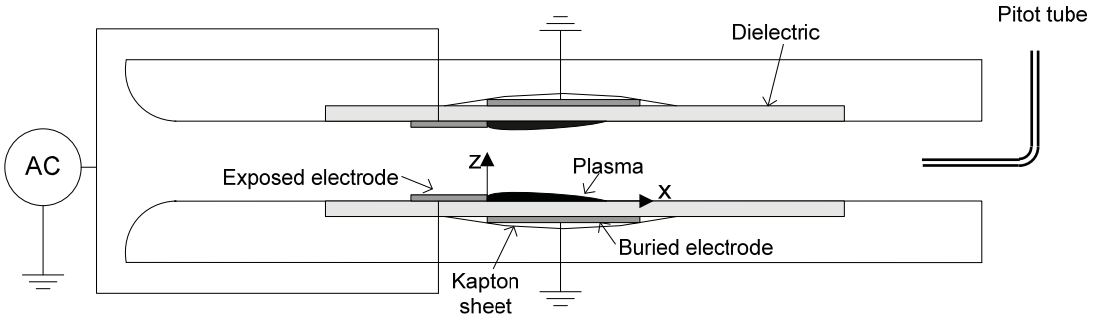

Figure 1. Schematic diagram of the experimental setup.

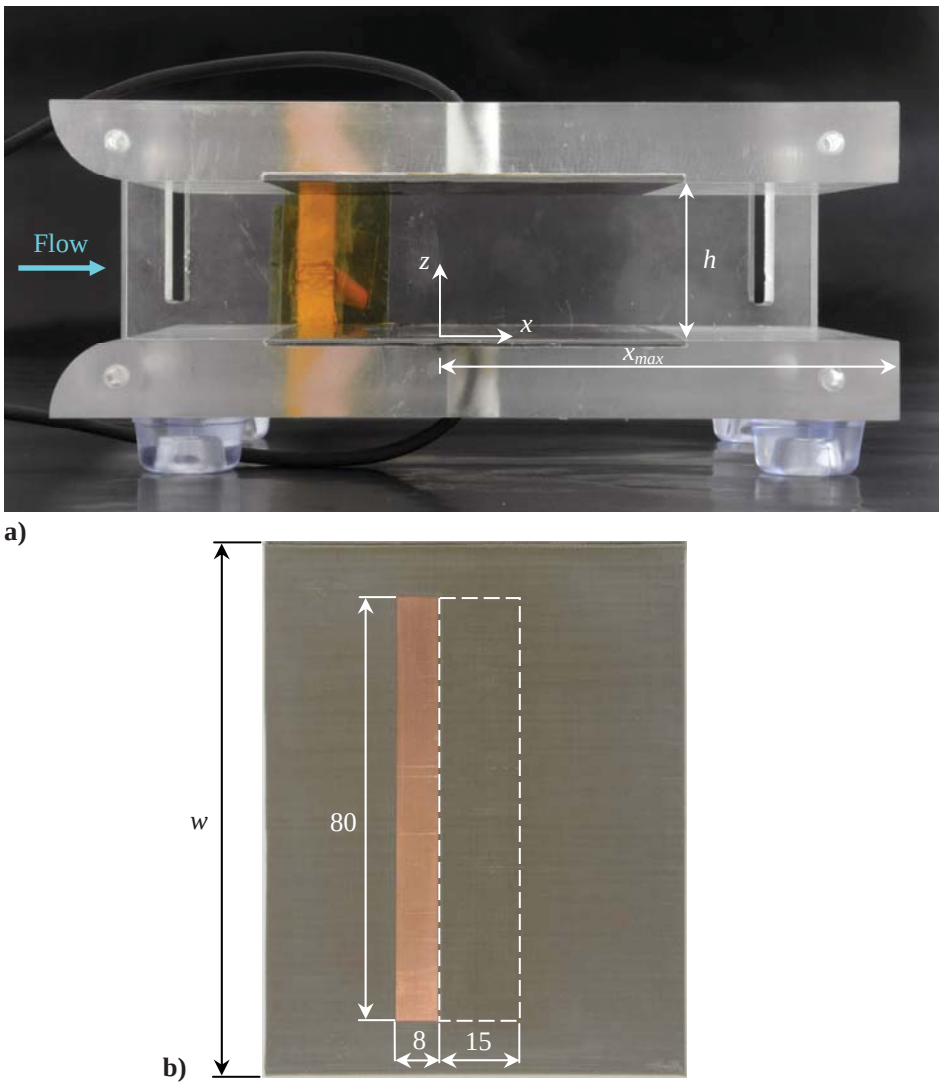

Figure 2. Pictures of the experimental setup. a) Side view of the DBD plasma channel. The side wall toward the camera has been removed to show the arrangement of the DBD actuators inside the channel. b)Top view of one DBD plasma actuator element. Visible is the copper exposed electrode; dashed lines indicate the size and position of the buried electrode; dimensions are in mm.

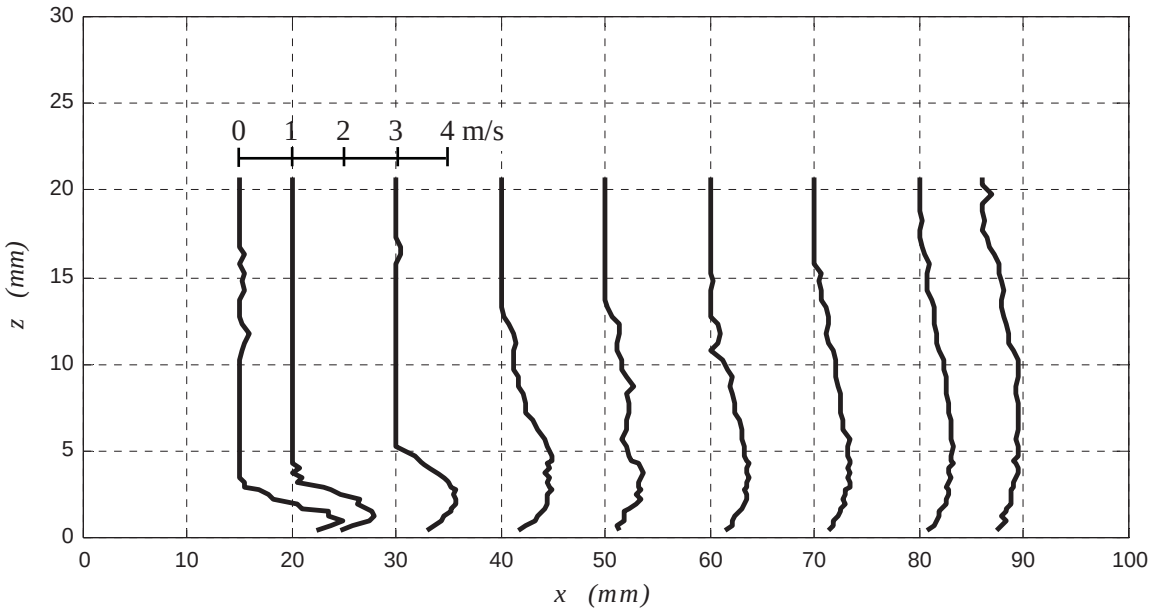

Figure 3. Flow velocity profiles *u*(*z*) measured at different distances *x* downstream of the exposed electrode for single (*h* = ∞) DBD plasma actuator operating at 8 kV_{pp}.

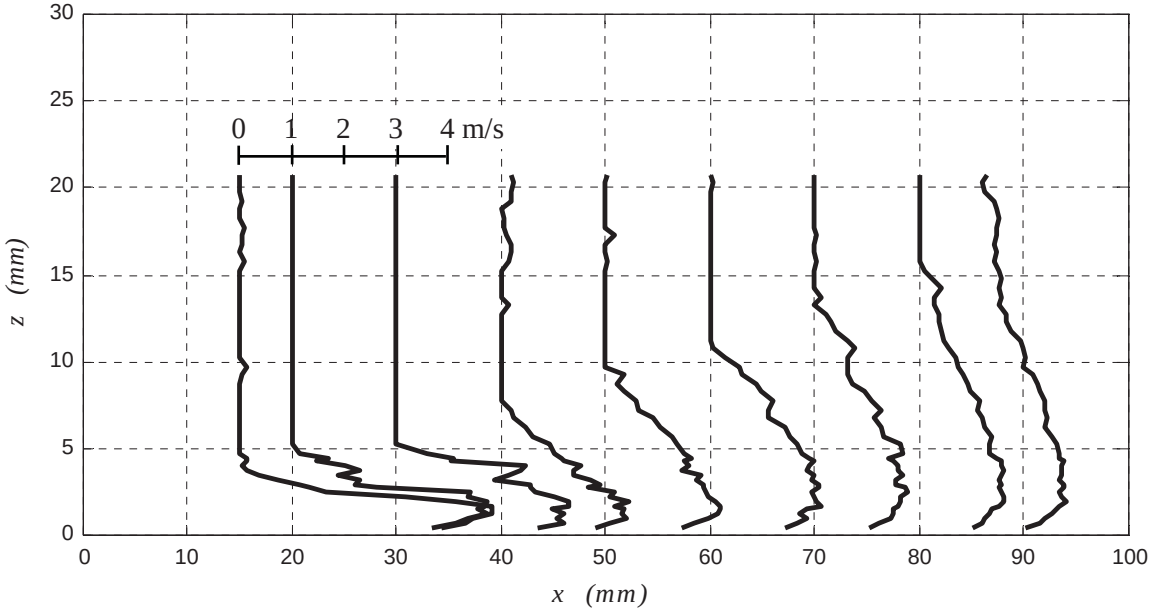

Figure 4. Flow velocity profiles *u*(*z*) measured at different distances *x* downstream of the exposed electrode for single (*h* = ∞) DBD plasma actuator operating at 12 kV_{pp}.

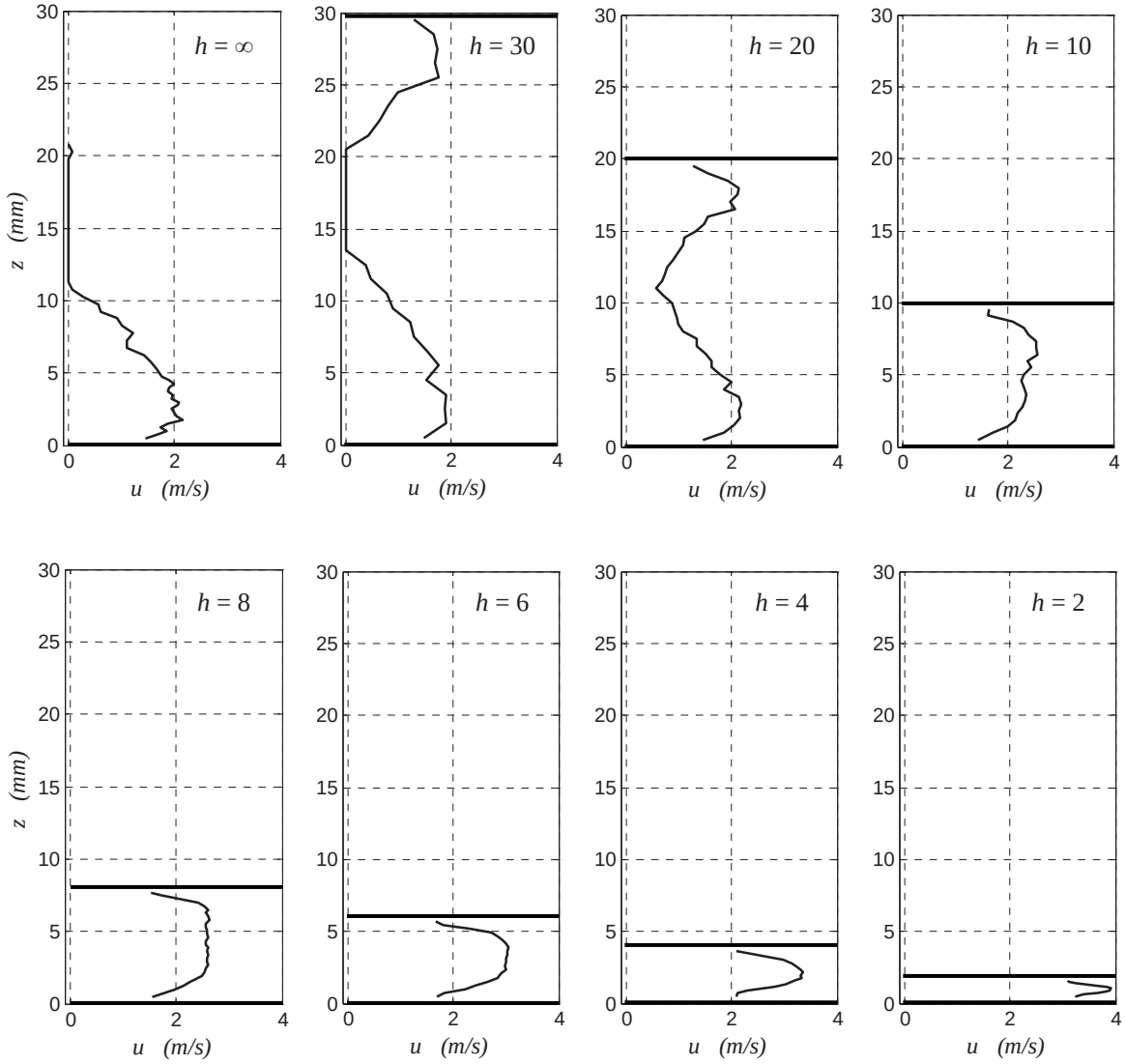

Figure 5. Flow velocity profiles *u*(*z*) measured for different values of the gap *h* (mm) at *x* = 63 mm downstream of the exposed electrodes for DBD plasma channel actuator operating at 12 kV_{pp}. Thick horizontal lines are used to visualize the position of the upper and lower walls of the channel.

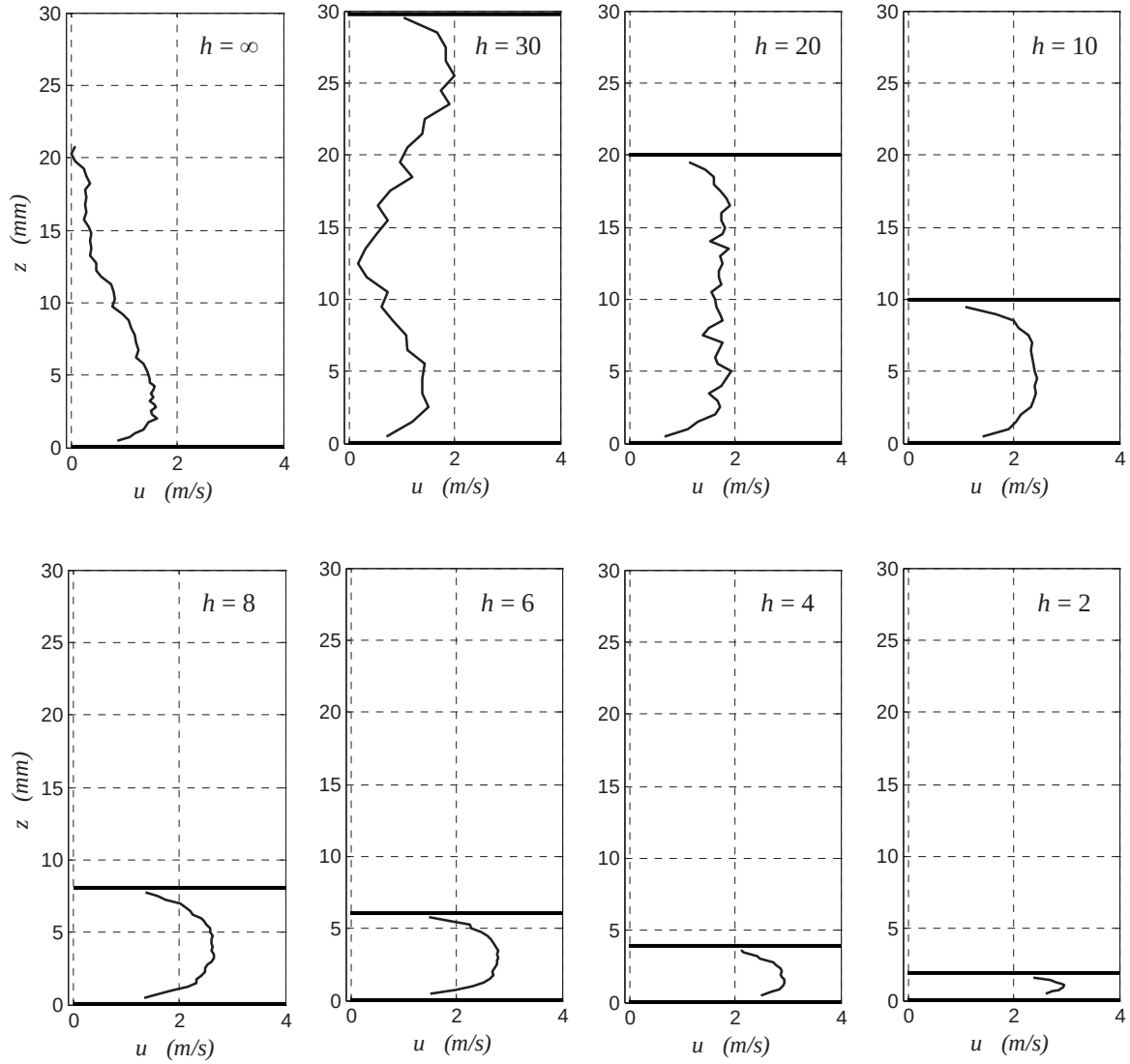

Figure 6. Flow velocity profiles *u*(*z*) measured for different values of the gap *h* (mm) at x_{max} = 86 mm downstream of the exposed electrodes for DBD plasma channel actuator operating at 12 kV_{pp}. Thick horizontal lines are used to visualize the position of the upper and lower walls of the channel.

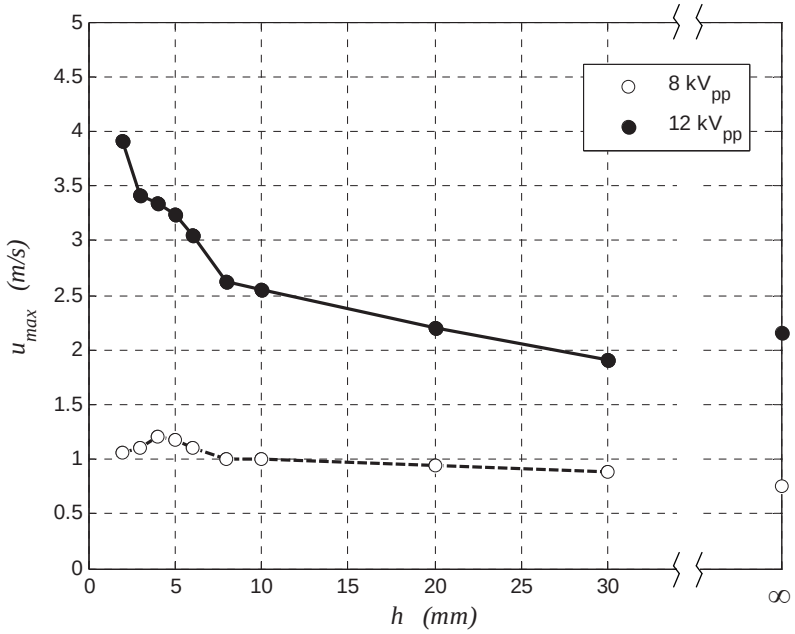

Figure 7: Maximum values of the flow velocity as a function of the channel height *h* measured at *x* = 63 mm downstream of the exposed electrodes.

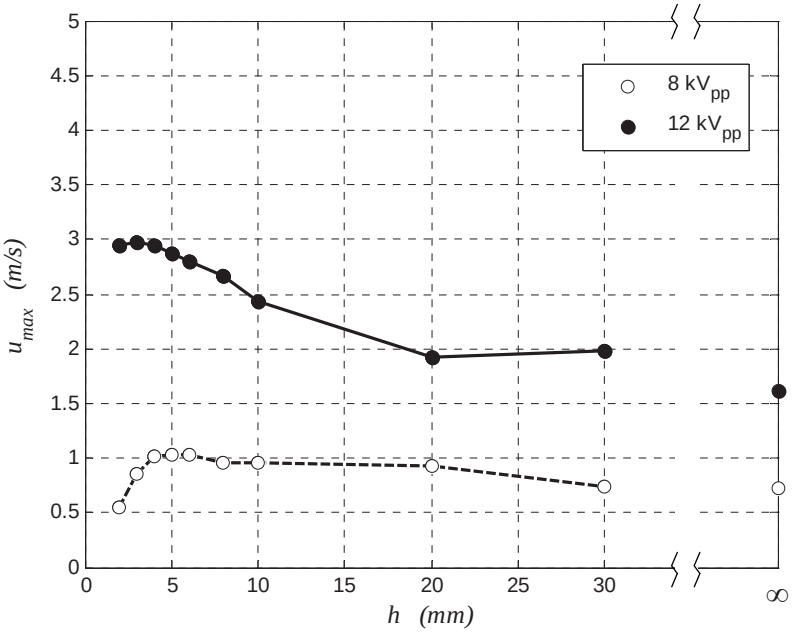

Figure 8: Maximum values of the flow velocity as a function of the channel height *h* measured at x_{max} = 86 mm downstream of the exposed electrodes.

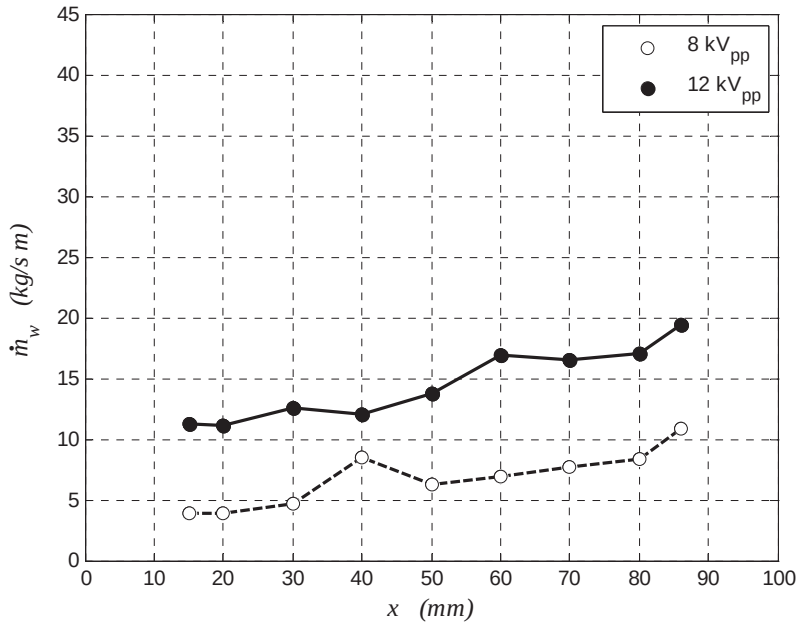

Figure 9: Mass flow rate per unit span of the wall jet created by single ($h = \infty$) DBD plasma actuator at different distances x downstream of the exposed electrode.

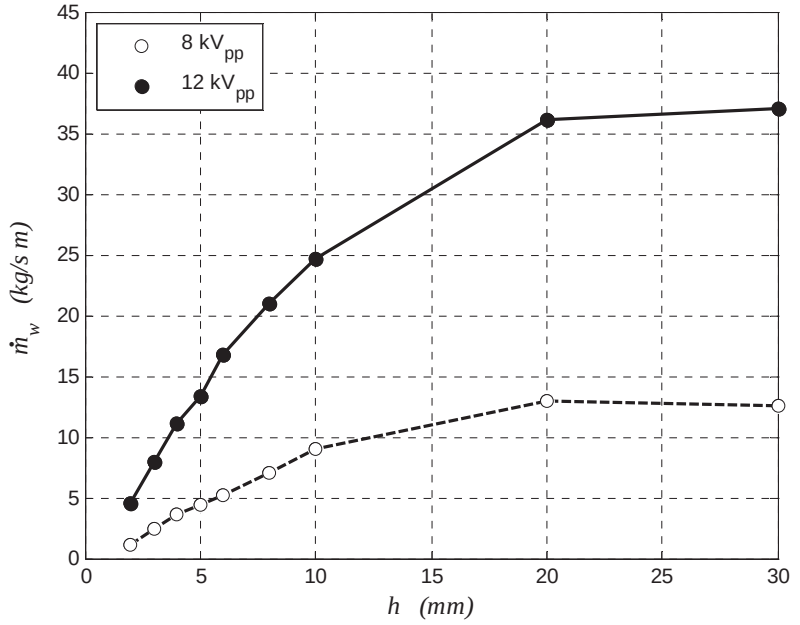

Figure 10: Mass flow rate per unit span of the channel flow as a function of the channel height h.

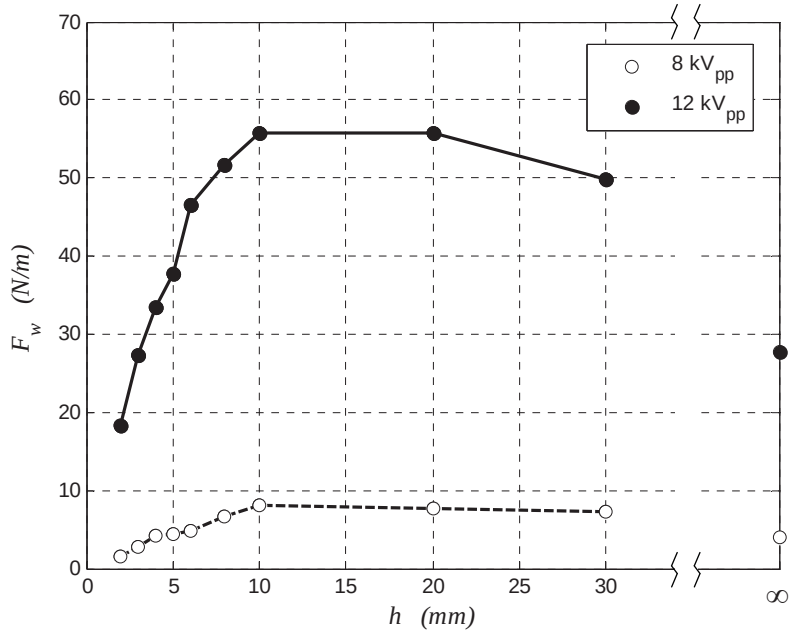

Figure 11: Force per unit span as a function of the channel height *h* measured at *x* = 63 mm downstream of the exposed electrodes.

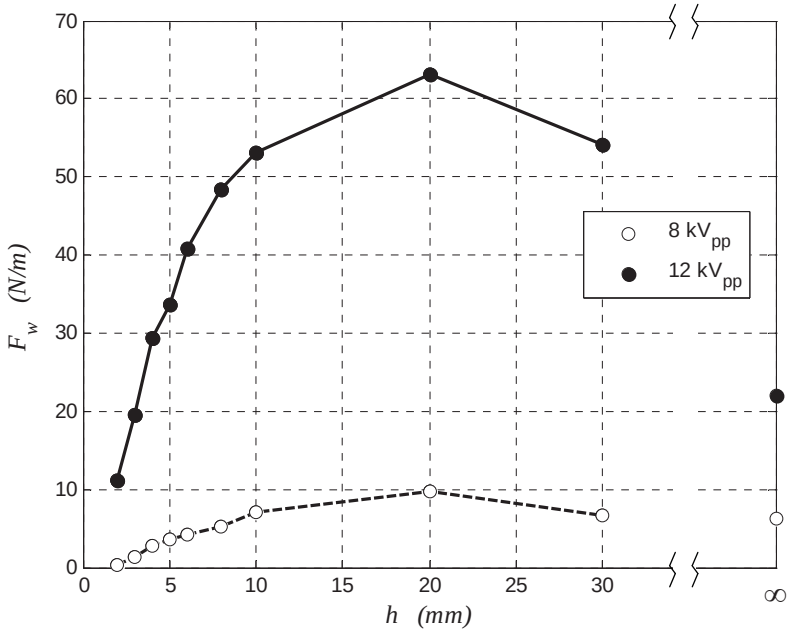

Figure 12: Force per unit span as a function of the channel height *h* measured at x_{max} = 86 mm downstream of the exposed electrodes.